Inorganic Chemistry

Article

pubs.acs.org/IC

Lower Denticity Leading to Higher Stability: Structural and Solution Studies of Ln(III)−OBETA Complexes

Roberto Negri,[†] Zsolt Baranyai,[‡] Lorenzo Tei,[§] Giovanni B. Giovenzana,*[,†] Carlos Platas-Iglesias,[∥] Attila C. Bényei,[⊥] Judit Bodnár,[‡,#] Adrienn Vágner,[‡] and Mauro Botta*[,§]

[†]Dipartimento di Scienze del Farmaco, Università degli Studi del Piemonte Orientale "A. Avogadro", Largo Donegani 2/3, I-28100 Novara, Italy

[‡]Department of Inorganic and Analytical Chemistry, University of Debrecen, Egyetem tér 1, H-4010 Debrecen, Hungary

[§]Dipartimento di Scienze e Innovazione Tecnologica, Università degli Studi del Piemonte Orientale "A. Avogadro", Viale T. Michel 11, I-15121 Alessandria, Italy

[∥]Departamento de Quimica Fundamental, Universidade de Coruña, Campus de Zapateira, Rúa da Fraga 10, 15008 A Coruña, Spain

[⊥]Department of Physical Chemistry, University of Debrecen, Egyetem tér 1, H-4010 Debrecen, Hungary

Supporting Information

ABSTRACT: The heptadentate ligand OBETA (2,2′-oxybis(ethylamine)-*N*,*N*,*N*′,*N*′-tetraacetic acid) was reported to form complexes with Ln^{3+} ions more stable than those formed by the octadentate and more popular congener EGTA (ethylene glycol *O*,*O*′-bis(ethylamine)-*N*,*N*,*N*′,*N*′-tetraacetic acid). The structural features leading to this puzzling coordination paradox were investigated by X-ray diffraction, solution state NMR, molecular modeling, and relaxometric studies. The stability constant of Gd(OBETA) (log K_{GdL} = 19.37, 0.1 M KCl) is 2 orders of magnitude higher than that of the higher denticity analogue Gd(EGTA) (log K_{GdL} = 17.66, 0.1 M KCl). The half-lives ($t_{1/2}$) for the dissociation reactions of Gd(OBETA) and Gd(EGTA) ($[Cu^{2+}]_{tot}$ = 0.2 mM, $[Cit^{3-}]_{tot}$ = 0.5 mM, $[PO_4^{3-}]_{tot}$ = 1.0 mM, and $[CO_3^{2-}]_{tot}$ = 25 mM at pH = 7.4 and 25 °C in 0.1 M KCl solution) are 6.8 and 0.63 h, respectively, reflecting the much higher inertness of Gd(OBETA) near physiological conditions. NMR studies and DFT calculations using the B3LYP functional and a large-core ECP indicate that the $[Gd(OBETA)(H_2O)_2]^-$ complex most likely exists in solution as the $\Delta(\lambda\lambda)(\delta\delta\delta\delta)_A/\Lambda(\delta\delta)(\lambda\lambda\lambda\lambda)_A$ enantiomeric pair, with an activation free energy for the enantiomerization process of ∼40 kJ·mol^{-1}. The metal ion is nine-coordinate by seven donor atoms of the ligand and two inner-sphere water molecules. The X-ray crystal structure of $[C(NH_2)_3]_3[Lu(OBETA)(CO_3)]\cdot 2H_2O$ is in agreement with the predictions of DFT calculations, the two coordinated water molecules being replaced by a bidentate carbonate anion. The ^{1}H NMRD and ^{17}O NMR study revealed that the two inner-sphere water molecules in Gd(OBETA) are endowed with a relatively fast water exchange rate (k_{ex}^{298} = 13 × 10^6 s^{-1}). The higher thermodynamic stability and inertness of Ln(OBETA) complexes, peaking in the center of the 4f series, combined with the presence of two coordinated water molecules suggests that Gd(OBETA) is a promising paramagnetic probe for MRI applications.

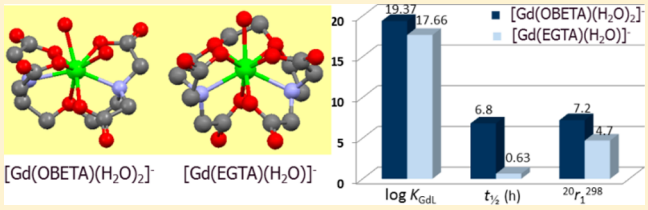

INTRODUCTION

MRI (magnetic resonance imaging) is one of the most evolved and sophisticated techniques used in clinical diagnostics and biomedical research as it provides 3D images of the body with high resolution.[1] Image contrast is often improved with the administration of a contrast agent (CA), generally a paramagnetic compound that accelerates the relaxation rate of the water molecules in the surrounding tissue.

Different families of CAs have been developed over the past 20 years, for example, nanoparticles, metal oxides, or complexes of Mn^{2+}, Fe^{3+}, or Gd^{3+}.[2] Among all these kinds of CAs, paramagnetic Gd^{3+} complexes are still the most widely used in the clinic. The real challenge for chemists developing Gd-based MRI probes is the extremely high stability which is necessary to prevent the release of the metal ion, which is toxic.[3] This requirement, usually associated with the utilization of octa- or nonadentate ligands, contrasts with the need for leaving space for one or more coordinated water molecules on the metal center, to attain high relaxivities, realized by ligands with lower denticities.[4] The compromise between stabilities and relaxivities is normally obtained with octadentate DOTA- or DTPA-like complexes (DOTA, 1,4,7,10-tetraazacyclododecane-1,4,7,10-tetraacetic acid; DTPA, diethylenetriaminepentaacetic acid), although properly designed ligands with lower denticity may combine excellent stability profiles with superior relaxivities for the corresponding Gd^{3+} complexes (Figure 1).[5,6]

Among the limited number of ligands with denticities lower than eight, the acyclic heptadentate ligand OBETA (2,2′-oxybis(ethylamine)-*N*,*N*,*N*′,*N*′-tetraacetic acid; Figure 1), pre-

Received: August 19, 2014
Published: November 11, 2014

   dx.doi.org/10.1021/ic5020225 | Inorg. Chem. 2014, 53, 12499−12511

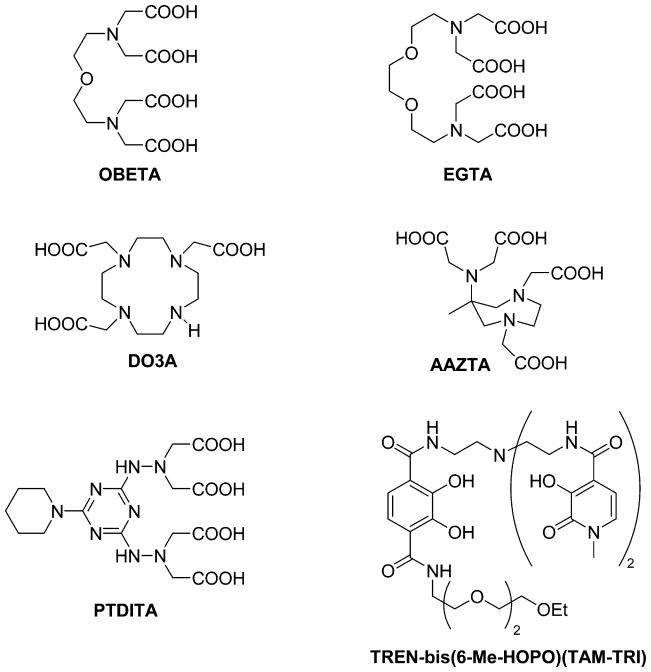

Figure 1. Chemical structures of OBETA, EGTA, and selected lower denticity chelating ligands discussed in this work.

pared for the first time more than 60 years ago, intrigued us for its high formation constants with lanthanide(III) ions.[7] In particular, the highest stability constant across the lanthanide series was measured for Gd^{3+}, which surprisingly is even higher than that of the corresponding complex with the better known octadentate analogue EGTA (Figure 1). Recently, we have redetermined the thermodynamic properties of selected Ln^{3+} complexes with more modern and accurate potentiometric techniques,[8] which provided stability constants somewhat higher than those reported previously.[7b] We also provided initial evidence of the inertness of Gd(OBETA) toward transmetalation reactions, a necessary property for a safe *in vivo* use of a metal complex. Finally, we performed a preliminary evaluation of the ^{1}H NMR relaxometric properties of $[Gd(OBETA)(H_2O)_2]^-$ to estimate its potential as an MRI contrast agent.

In this paper, we report a detailed investigation of the structural features underlying the unusually high stability of Ln^{3+}–OBETA complexes with respect to the corresponding EGTA congener; a combination of X-ray crystallography, solution state NMR, and molecular modeling sheds light on their critical structural differences. A full account of the solution thermodynamics of the chelates of OBETA with several metal ions is provided, along with a detailed kinetic study of their principal dissociation pathways. Finally, the relaxometric properties of $[Gd(OBETA)(H_2O)_2]^-$ were investigated in aqueous solution by measuring the dependence of the ^{1}H relaxivity on magnetic field strength. Information on the water exchange dynamics was also obtained from analysis of the temperature dependence of the water ^{17}O NMR transverse relaxation rate (R_2) and chemical shift ($\Delta\omega$) data.

RESULTS AND DISCUSSION

Protonation and Complexation Equilibria of OBETA. *Protonation Equilibria of the OBETA Ligand.* The ligand protonation constants were determined by pH potentiometry[8] and ^{1}H NMR spectroscopy (Table 1 and Figure S1 in the Supporting Information). The equations used for the evaluation

Table 1. Protonation Constants (log K_i^H) and Total Basicity ($\sum$log K_i^H) for OBETA and EGTA (0.1 M KCl, 25°C)[a]

	OBETA			EGTA	
	^{1}H NMR	pH pot.[b]	pH pot.[c]	pH pot.[b]	pH pot.[c]
	0.1 M KCl	0.1 M KCl	0.1 M KNO_3	0.1 M KCl	0.1 M KNO_3[c]
log K_1^H	9.5 (1)	9.34	9.39	9.43	9.47
log K_2^H	8.8 (1)	8.62	8.75	8.82	8.85
log K_3^H	2.9 (1)	3.19	2.76	2.77	2.66
log K_4^H	2.0 (1)	2.19	1.80	2.06	2.00
log K_5^H		1.77		1.88	
$\sum_{i=1}^{4}$ log K_i^H	23.20	23.34	22.70	23.08	22.98

[a]Standard deviations are shown in parentheses. [b]Reference 8. [c]Reference 7b.

of the protonation constants and the ^{1}H NMR studies of the protonation process of OBETA are summarized in the Supporting Information. The comparison between OBETA and EGTA reveals that log K_1^H and log K_4^H are quite similar, whereas log K_2^H is slightly lower and log K_3^H is higher for OBETA than for EGTA. The lower second protonation constant for OBETA can be explained by the shorter ligand backbone resulting in an increased electrostatic repulsion between the protonated nitrogen atoms. Although the log K_i^H values obtained from the ^{1}H NMR study are in good agreement with the pH potentiometry data, the experimental error is relatively large because the protonation constants of similar donor atoms cannot be evaluated independently due to the concomitant protonation processes.

Complexation Properties of OBETA and EGTA. As already noted above, the stability constants of both OBETA and EGTA with selected lanthanide(III) and transition metal ions were reported several decades ago.[7b] Together with the redetermination of these data by pH potentiometry and UV–vis spectrophotometry for the Ln(OBETA) complexes, we decided to also collect new data for EGTA using identical experimental conditions (25 °C, 0.1 M KCl), to gain reliable and accurate data for comparison of the two ligands (Table 2).

According to the $\sum_{i=1}^{4}$ log K_i^H values reported in Table 1, the stability constants of the OBETA complexes are expected to be comparable to those of the corresponding EGTA complexes. Despite this and the higher denticity of EGTA, the stability constants of the OBETA complexes are generally about 1–2 orders of magnitude higher than those of the corresponding EGTA complexes (Table 2). This can be explained by the shorter ligand backbone of the 2,2′-oxybis(ethylamine) moiety that results in a more compact and stronger coordination of all donor atoms to the mid-sized lanthanide(III) ions. Also, the lower flexibility of the complexes might play an important role due to a better size match between the metal ion and the coordination cage of the ligand. To support this hypothesis, it is noteworthy that the log K_{ML} values of Lu(OBETA) and Ca(OBETA) are about 1 order of magnitude lower than those of the corresponding EGTA complexes, probably due to a mismatch between the small ionic radius of Lu^{3+} and Ca^{2+} and the compact coordination cage formed by the donor atoms of the OBETA ligand.

Considering the trend in the stability constants across the lanthanide series, it can be highlighted that for the Ln(OBETA)

dx.doi.org/10.1021/ic5020225 | Inorg. Chem. 2014, 53, 12499–12511

Table 2. Stability and Protonation Constants of the Complexes Formed with OBETA and EGTA (25°C)[a]

	OBETA			EGTA			DTPA[b]
	0.1 M KCl		0.1 M KNO_3[c]	0.1 M KCl		0.1 M KNO_3[c]	0.1 M KCl
	ML	MHL	ML	ML	MHL	ML	ML
Mg^{2+}	7.95 (2)		8.37[d]	5.26 (1)	7.86 (2)	5.28[d]	9.27
Ca^{2+}	9.77 (3)		9.92[d]	10.65 (1)	4.24 (2)	10.86[d]	10.75
Mn^{2+}	13.57(2)	3.45(6)	13.7[d]	12.28 (3)	4.43 (3)	12.2[d]	15.2
La^{3+}	16.89[e]	2.85[e]	16.29	15.60[e]	2.39[e]	15.84	19.48
Ce^{3+}	17.34 (2)	2.53 (2)	17.13	15.87 (2)	2.35 (1)	16.06	20.5
Nd^{3+}	18.39[e]	2.37[e]	17.81	16.77[e]	2.31[e]	16.59	21.6
Sm^{3+}	19.02 (1)	2.22 (1)	18.25	17.66 (1)	2.03 (1)	17.25	22.35
Eu^{3+}	19.13 (1)	2.21 (1)	18.38	17.70 (1)	1.95 (2)	17.77	22.39
Gd^{3+}	19.37 (1)	2.20 (1)	18.21	17.66 (1)	1.89 (1)	17.50	22.46
Dy^{3+}	18.87 (1)	2.28 (1)	18.29	18.02 (1)	1.77 (2)	17.84	22.82
Ho^{3+}	18.93[e]	2.29[e]	18.17	18.1[e]	1.79[e]	17.90	22.79
Er^{3+}	18.46 (2)	2.23 (2)	18.18	17.98 (1)	1.56 (3)	18.00	22.74
Yb^{3+}	18.31 (1)	2.30 (1)	18.06	18.33 (1)	1.35 (3)	18.22	22.62
Lu^{3+}	17.93[e]	2.42[e]	17.92	18.67[e]	1.47[e]	18.48	22.44

	Cu^{2+}		Zn^{2+}		Cu^{2+}		Zn^{2+}		Cu^{2+}	Zn^{2+}
	0.1 M KCl	0.1 M KNO_3[d]	0.1 M KCl	0.1 M KNO_3[d]	0.1 M KCl	0.1 M KNO_3[d]	0.1 M KCl	0.1 M KNO_3[d]	0.15 M NaCl[f]	0.15 M NaCl[f]
ML	18.40 (4)	18.0	15.00 (1)	15.2	17.22 (2)	17.70	12.65 (2)	12.6	23.4	17.6
MHL	3.71 (2)	4.22	3.18 (1)	2.75	4.38 (1)	4.28	5.03 (1)	4.96	4.63	5.37
MH_2L	2.05 (2)				2.16 (2)		2.57 (2)		2.67	2.38
M_2L	5.74 (3)		2.05 (1)		5.90 (3)	4.18	3.23 (3)	3.3	6.56	4.33
M_2LH_{-1}	6.42 (1)				6.71 (5)	6.95	6.77 (4)			
M_2LH_{-2}	8.56 (6)				7.43 (5)	8.05				

[a]The experimental details and the equations used for the evaluation of the equilibrium data are provided in the Supporting Information. [b]Reference 10. [c]Reference 7b. [d]Reference 9. [e]Reference 8. [f]Reference 11. Ln(OBETA): log $K_{LaLH_{-1}}$ = 11.53 (4), log $K_{CeLH_{-1}}$ = 11.89 (6). Mn(EGTA): log K_{MH_2L} = 4.13 (3) by pH potentiometry (0.1 M KCl, 25 °C). Cu(OBETA): log K_{ML} = 18.89 (3) by spectrophotometry (0.1 M KCl, 25 °C).

complexes there is an increase in the log K_{LnL} from La^{3+} to Gd^{3+} followed by a smoother decrease for the late members of the series (Figure 2 and Table 2), whereas for Ln(EGTA) the

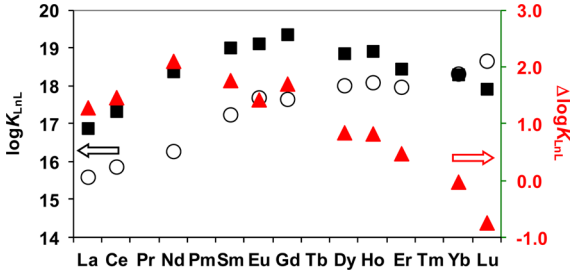

Figure 2. Stability constants (log K_{LnL}) and Δlog K_{LnL} (red ▲) of the Ln(OBETA) (black ■) and Ln(EGTA) (black ○) complexes (Δlog K_{LnL}= log $K_{Ln(OBETA)}$ − log $K_{Ln(EGTA)}$).

log K_{LnL} values steadily increase across the series from La^{3+} to Lu^{3+}. The stability trend observed for the Ln(EGTA) complexes simply reflects an increasing binding energy of the ligand to the metal ion along the series as a consequence of the increased charge density of the cation. The log K_{LnL} values of Ln(DTPA) complexes increase from La^{3+} to Dy^{3+} and then remain practically constant for the heavier lanthanide(III) ions with a slight decrease in the end of the series, accounted for by the electrostatic repulsion between the negatively charged carboxylate groups with the smaller lanthanide(III) ions.[10] In the case of the Ln(OBETA) complexes the coordination sites offered by the ligand are better suited for the large Ln^{3+} ions, which results in a drop in the stability constants for the heavier Ln^{3+} ions.[12] As a result, the Δlog K_{LnL} value between the complexes formed by the two ligands with the same Ln^{3+} ion shows a maximum for Nd^{3+} and then it decreases along the series until the situation is reversed (Yb^{3+} and Lu^{3+}). The general preference of lanthanide(III) ions for OBETA and, in particular, the optimal coordination match with Gd^{3+} are of particular interest for MRI applications since Gd^{3+} is the metal ion of choice and the chelating agent must form a highly stable complex to prevent *in vivo* dissociation.

Finally, both the Ln(OBETA) and Ln(EGTA) complexes can be protonated at low pH values, and their protonation constants were determined by pH potentiometry (Table 2). The OBETA complexes with Mn^{2+}, Zn^{2+}, and Cu^{2+} ions likely embody one or two noncoordinated or weakly coordinated donor atoms (carboxylate-O), which can be protonated at pH values around 3−4. On the other hand, in the Ln(OBETA) complexes all the carboxylate groups are strongly coordinated to the metal ion and thus their protonation occurs at more acidic pH (log K_{LnHL} = 2.2−2.9).

Dissociation Kinetics of Gd(OBETA) and Gd(EGTA) in the Presence of Endogenous Ligands. The importance of Gd^{3+} chelates in MRI and the unexpectedly high thermodynamic stability of Gd(OBETA) prompted us to explore its inertness in greater detail. The kinetic studies of the metal exchange reactions of Gd(OBETA) and Gd(EGTA) with Cu^{2+} or Zn^{2+} ions indicate that the transmetalation reactions take place through a very slow dissociation of the complexes via proton- and metal-assisted pathways. Although the dissociation may occur by proton assistance, in the pH range 6−8 this

dx.doi.org/10.1021/ic5020225 | Inorg. Chem. 2014, 53, 12499−12511

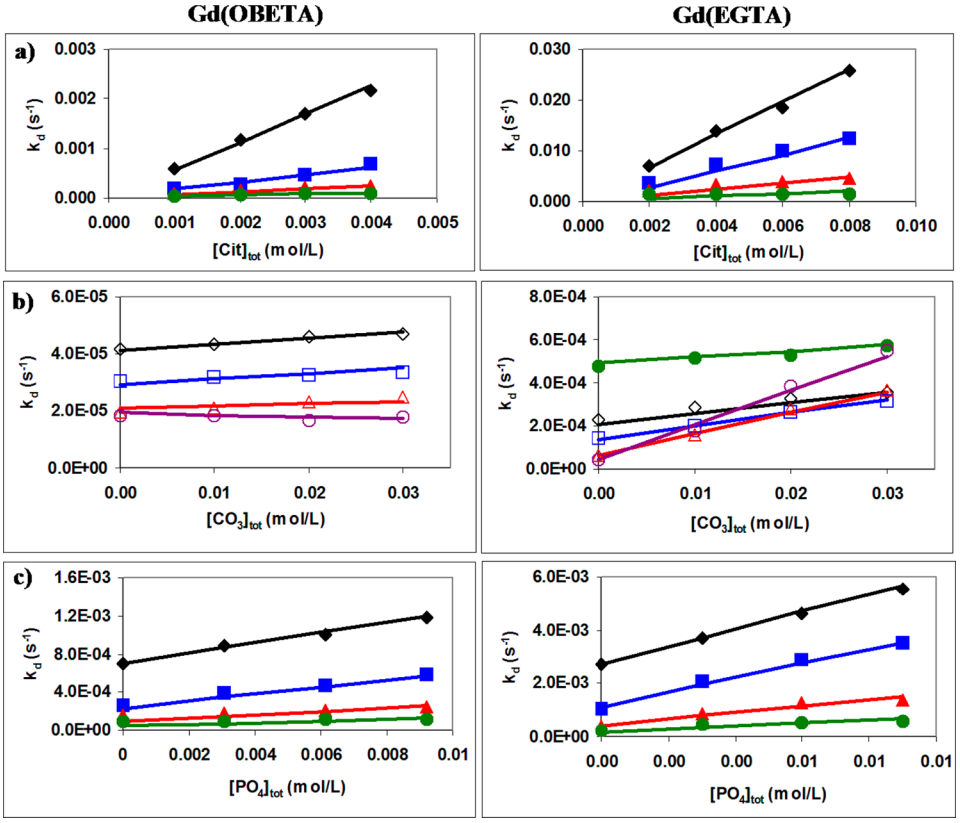

Figure 3. Dependence of the k_d rate constants on the total citrate (a), carbonate (b), and phosphate (c) concentration for the reaction of Gd(OBETA) (left) and Gd(EGTA) (right) with Cu^{2+} in the presence of citrate. (a) [Gd(EGTA)] = 6.0 mM, [Cu^{2+}] = 0.3 mM; [Gd(OBETA)] = 1.0 mM, [Cu^{2+}] = 0.1 mM. (b) [Gd(EGTA)] = 6.0 mM, [Cu^{2+}] = 0.3 mM, [Cit] = 1.0 mM; [Gd(OBETA)] = 1.0 mM, [Cu^{2+}] = 0.1 mM, [Cit] = 2.0 mM. (c) [Gd(EGTA)] = 2.0 mM, [Cu^{2+}] = 0.3 mM, [Cit] = 1.0 mM; [Gd(OBETA)] = 1.0 mM, [Cu^{2+}] = 0.2 mM, [Cit] = 2.0 mM. pH = 6.0 (black ◆), 6.5 (blue ■), 7.0 (red ▲), 7.5 (green ●), 8.0 (black ◇), 8.5 (blue □), 9.0 (red △), and 9.5 (purple ○); 0.1 M KCl and 25 °C.

Table 3. Rate (k) and Equilibrium (K) Constants and Half-Lives ($t_{1/2}$ = ln 2/k_d) for the Dissociation of Gd(OBETA) and Gd(EGTA) in the Presence of Citrate, Carbonate, and Phosphate Ions (0.1 M KCl, 25°C)

	Gd(OBETA)	Gd(EGTA)	Gd(DTPA)[b]
k_1 (M^{-1} s^{-1})	7.8[a]	60[a]	0.58[c]
k_{Cit} (M^{-1} s^{-1})	(1.3 ± 0.3) × 10^{-2}	(7 ± 1) × 10^{-2}	4.4 × 10^{-5}
k_{HCit} (M^{-1} s^{-1})	1.05 ± 0.13	11 ± 1	7.7 × 10^{-3}
k_{HHCit} (M^{-1} s^{-1})	18.1 ± 1.2		
k_{CO_3} (M^{-1} s^{-1})		(4.4 ± 0.7) × 10^{-2}	3.1 × 10^{-4}
k_{HCO_3} (M^{-1} s^{-1})	(3.5 ± 0.9) × 10^{-4}	(5.5 ± 0.8) × 10^{-3}	2.2 × 10^{-5}
$k_{H_2PO_4}$ (M^{-1} s^{-1})	(5.5 ± 0.7) × 10^{-2}	0.19 ± 0.03	2.7 × 10^{-4}
k_{HMES} (M^{-1} s^{-1})		(7 ± 1) × 10^{-2}	
k_{HHEPES} (M^{-1} s^{-1})		(1.0 ± 0.1) × 10^{-2}	
K_{GdHL} (M^{-1})	158.5 (pH pot.)	78 (pH pot.)	100[c]
K_{GdLCO_3} (M^{-1})	100 ± 14		
k_d (s^{-1})	2.8 × 10^{-5}	3.0 × 10^{-4}	6.3 × 10^{-7}
$t_{1/2}$ (h)	6.8	0.63	307

[a]Reference 8. [b]Reference 13. [c]Reference 14.

pathway is much slower than the measured reaction rates: $k_d \gg k_1[H^+]$, where k_1 is the rate constant for the proton assisted dissociation of the complexes.[8] Therefore, to further investigate the kinetics of dissociation near physiological conditions, we studied the transmetalation reaction with Cu^{2+} following the model exchange reaction 1. The experiments were carried out in the pH range 6.0−9.5 and in the presence of citrate ions (Cit), in order to avoid precipitation of both the Cu^{2+} and the released Gd^{3+} ions. The transmetalation reactions essentially take place between Gd(OBETA) or Gd(EGTA) and Cu(Cit)-H_{-1}, as, in the presence of an excess of citrate, Cu^{2+} is predominantly present as a monomeric complex species.[13]

$$GdL + Cu^{2+}\ \text{citrate} \rightleftharpoons Gd^{3+}\ \text{citrate} + CuL \quad (1)$$

Moreover, the rates of the exchange reaction 1 were studied in the absence and presence of HCO_3^-/CO_3^{2-} and phosphate ions by spectrophotometry in the pH range 6.0−9.5. The dependence of the pseudo first order rate constants (k_d) for the

dx.doi.org/10.1021/ic5020225 | Inorg. Chem. 2014, 53, 12499−12511

transmetalation reactions of Gd(OBETA) and Gd(EGTA) with Cu^{2+} as a function of citrate, HCO_3^-/CO_3^{2-}, and phosphate concentrations are shown in Figure 3a–c. The definitions and equations used for the evaluation of the kinetic data are provided in the Supporting Information.

The data presented in Figure 3a indicate that, at constant $[Cu^{2+}]$, the rates of the reaction increase with increasing citrate concentration. In the pH range 6–8 citrate is present as H_2Cit^-, $HCit^{2-}$, and Cit^{3-} species (log K_1^H = 5.70 (1), log K_2^H = 4.36 (1), log K_3^H = 2.92 (1), 0.1 M KCl, 25 °C). To interpret the trend in the k_d values, we assumed that in reaction 1 H_2Cit^-, $HCit^{2-}$, and Cit^{3-} catalyze the dissociation of Gd(OBETA) or Gd(EGTA), as characterized by the rate constants, k_{HCit} and k_{Cit}, respectively (Table 3).

In Figure 3b, the rate of the transmetalation reaction of Gd(EGTA) slightly increases with the increase in total concentration of carbonate ion at pH = 7.5 and 8.0, whereas at pH = 9.0 and 9.5 the increase of the k_d values is significantly larger. By taking into account the protonation constants of the carbonate ion (log K_1^H = 9.95(1), 0.1 M KCl, 25 °C), it can be assumed that both HCO_3^- and CO_3^{2-} ions catalyze the dissociation reactions of Gd(EGTA). On the other hand, the k_d values of Gd(OBETA) slightly increase with the increase in total carbonate concentration at pH = 8.0 and pH = 8.5 (HCO_3^- species) and decrease at pH > 9.0, where the CO_3^{2-} ion predominates. This small decrease at basic pH can be explained by the interaction of Gd(OBETA) with CO_3^{2-} and the formation of a ternary Gd(OBETA)CO_3 complex characterized by a slower dissociation rate. The structure of this ternary complex may likely resemble the structure of $[Lu(OBETA)(CO_3)]^{3-}$ reported below with an η^2-CO_3^{2-} coordination, compatible with a slower dissociation rate. The rate constants characterizing the HCO_3^- and CO_3^{2-} assisted dissociation reactions of Gd(OBETA) and Gd(EGTA) are k_{HCO_3} and k_{CO_3}, respectively (Table 3).

Phosphate ions also increase the rate of the exchange reaction 1 (Figure 3c), but the pH dependence of the k_d values is somewhat different from that observed for the carbonate ions. The slope of the straight line showing the dependence of k_d with $[PO_4]_{tot}$ is greater at pH ≈ 6 and lower at pH ≈ 7.5–8.0. As indicated by the protonation constants of the phosphate ion (log K_1^H = 11.64 (1), log K_2^H = 6.71 (1), log K_3^H = 1.84 (1), 0.1 M KCl, 25 °C), the species $H_2PO_4^-$ predominates at pH = 6, while HPO_4^{2-} ion is predominant at pH ≥ 7.5. Thus, it can be inferred that the critical role in the increase of the k_d values with increasing $[PO_4]_{tot}$ is played by $H_2PO_4^-$ ions and therefore the rate constant characterizing the effect of $H_2PO_4^-$ ion is $k_{H_2PO_4}$ (Table 3).

For Gd(EGTA), the effect of 2-(*N*-morpholino)-ethanesulfonic acid (MES) and 4-(2-hydroxyethyl)-1-piperazineethanesulfonic acid (HEPES) buffers used during the kinetic measurements must be also taken into account to obtain an accurate analysis of the data. In fact, the rates of the transmetalation reactions between Gd(EGTA) and Cu^{2+} ion increase with an increase in $[MES]_{tot}$ and $[HEPES]_{tot}$ at pH = 6.0, 6.5, and 7.0, respectively (Figure S8 in the Supporting Information). Considering the protonation constants of MES and HEPES buffers (MES, log K_1^H = 6.02(1); HEPES, 7.31(1), 0.1 M KCl, 25 °C), it is assumed that the protonated form of MES and HEPES buffers can accelerate reaction 1 for Gd(EGTA). On the other hand, the metal exchange reactions of Gd(OBETA) with Cu^{2+} ion are not affected by buffers.

The data reported highlight that H_2Cit^-, $HCit^{2-}$, Cit^{3-}, HCO_3^-, CO_3^{2-}, and $H_2PO_4^-$ ions catalyze the dissociation of Gd(OBETA) and Gd(EGTA) via the formation of ternary complexes. The stability constant for Gd(OBETA)(CO_3^{2-}) was calculated from the kinetic data as $K_{Gd(L)CO_3}$ = 100 ± 14 M^{-1} (log $K_{Gd(L)CO_3}$ = 2.0(1)). Finally, by taking into account the rate and equilibrium constants presented in Table 3, the k_d rate constants and the half-life ($t_{1/2}$) values for the dissociation reactions of Gd(OBETA) and Gd(EGTA) were calculated using the following conditions: $[Cu^{2+}]_{tot}$ = 0.2 mM, $[Cit^{3-}]_{tot}$ = 0.5 mM, $[PO_4^{3-}]_{tot}$ = 1.0 mM, and $[CO_3^{2-}]_{tot}$ = 25 mM at pH = 7.4 and 25 °C in 0.1 M KCl solution (Table 3).

The calculated rate constants show that the dissociation of Gd(EGTA) in the presence of citrate, carbonate, and phosphate ions occurs 2–10 and 100 times faster than for Gd(OBETA) and for Gd(DTPA), respectively. In order to confirm k_d and $t_{1/2}$, the transmetalation reactions between Gd(OBETA) (2.0 mM), Gd(EGTA) (2.0 mM), or Gd(DTPA) (2.0 mM) and Cu^{2+} (0.2 mM) were followed by spectrophotometric techniques in the presence of 0.5 mM citrate, 1.0 mM phosphate, 25 mM CO_3^{2-}, and 10 mM HEPES, at pH = 7.4 and 25 °C in 0.1 M KCl. The plots of the absorbance at 300 nm vs time gave straight lines (Figure S9 in the Supporting Information), from which the k_d rate constants were calculated (eq 11 in the Supporting Information) to be 3.1×10^{-5} s^{-1} ($t_{1/2}$ = 6.2 h) for Gd(OBETA), 2.9×10^{-4} s^{-1} ($t_{1/2}$ = 0.66 h) for Gd(EGTA), and 6.5×10^{-7} s^{-1} ($t_{1/2}$ = 296 h) for Gd(DTPA). The molar absorptivity of Cu(DTPA) ($\varepsilon_{Cu(DTPA)}$ (300 nm) = 3969 M^{-1} cm^{-1})[13] was used to calculate the k_d rate constant of Gd(DTPA). The k_d and $t_{1/2}$ values obtained experimentally and by calculation (Table 3) are in good agreement, and therefore we can safely conclude that the k_{Cit}, k_{HCit}, k_{CO_3}, k_{HCO_3}, $k_{H_2PO_4}$, and k_{HHEPES} rate constants are reliable and can be used to calculate the dissociation rates of Gd(OBETA), Gd(EGTA), and Gd(DTPA).

The mechanism of the transmetalation reaction of Gd(OBETA) and Gd(EGTA) with Cu^{2+} may be accounted for by a catalyzing effect of citrate, carbonate, and phosphate ions in the dissociation of the Gd^{3+} complexes, followed by a fast reaction between the Cu(Cit)H_{-1} species and the free ligand. The effect of the anions on the rate of dissociation of Gd(EGTA) or Gd(OBETA) can be interpreted in terms of the following: (i) a proton transfer from the protonated citrate, carbonate, or phosphate ions to the carboxylate group of the metal complexes (general acid catalysis); (ii) a faster isomerization of the ternary adduct formed by Gd(OBETA) or Gd(EGTA) and the anions due to the electrostatic repulsion between the negatively charged donor atoms. To distinguish between the two possible dissociation pathways, the k_X rate constants (X = H_2Cit^-, $HCit^{2-}$, HCO_3^-, $H_2PO_4^-$) of Gd(OBETA) and Gd(EGTA) (X also indicates HMES and HHEPES for Gd(EGTA)) were plotted as a function of the protonation constants (log K_X^H) of the related ions. In Figure 4, the k_X rate constants characterizing the protonated-ion assisted dissociation of Gd(OBETA) decrease monotonously with the increase in the protonation constants of the ions, highlighting the key role of the protonated ions in the dissociation of the metal complex. The rate of the proton catalyzed reactions is accelerated by general acids, and the k_X rate constants are directly proportional to the acid strength (log K_X^H; log $k_X = \alpha \times \log K_X^H + C$).[15] The Brønsted plot of the pure proton transfer reactions are characterized by straight lines

dx.doi.org/10.1021/ic5020225 | Inorg. Chem. 2014, 53, 12499–12511

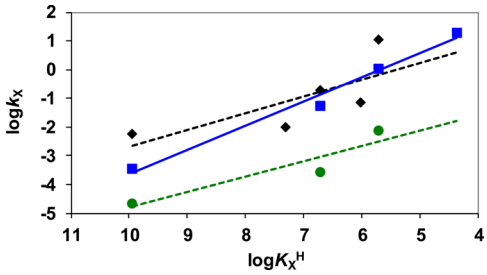

Figure 4. Brønsted plot for the dissociation reaction of Gd(OBETA) (blue squares), Gd(EGTA) (black diamonds), and Gd(DTPA) (green circles) assisted by H_2Cit^-, $HCit^{2-}$, HCO_3^-, $H_2PO_4^-$, HMES, and HHEPES ions (0.1 M KCl, 25 °C).

with $\alpha = 1.0$.[15] Since for Gd(OBETA) $\alpha = 0.84 \pm 0.07$, we can assume that its dissociation takes place predominantly by the general acid catalyzed pathway through proton transfer from the protonated H_2Cit^-, $HCit^-$, HCO_3^-, and $H_2PO_4^-$ anions to OBETA in the ternary Gd(OBETA)X adducts.

The k_X rate constants of Gd(EGTA) slightly decrease with an increase in the log K_X^H values of the ions, even if the log k_X values of Gd(EGTA) generally show large deviations from linearity in the Brønsted plot. This suggests that the dissociation of Gd(EGTA) not only takes place through the general acid catalyzed pathway but, at least partially, may occur via the formation of ternary complexes with anions, followed by a fast isomerization and dissociation of the complex. Interestingly, the slopes of the Brønsted plot obtained for Gd(EGTA) and Gd(DTPA) are very similar, which indicates that the dissociation mechanisms of both complexes are also similar (Figure 4). In the presence of endogenous ligands the dissociation of Gd(DTPA) occurs via the formation of ternary complexes, which can accelerate intramolecular rearrangements that favor the dechelation reactions. Indeed, ^{1}H and ^{13}C NMR spectroscopy studies showed that the presence of citrate, phosphate, and carbonate ions increase the rates of intramolecular rearrangements of Y(DTPA).[13]

X-ray Structure of $[C(NH_2)_3]_3[Lu(OBETA)(CO_3)]\cdot 2H_2O$. Single crystals of formula $[C(NH_2)_3]_3[Lu(OBETA)(CO_3)]\cdot 2H_2O$ suitable for X-ray diffraction studies were grown from an aqueous solution of the Lu^{3+} complex of OBETA in the presence 2.0 molar equiv of guanidinium carbonate ($[C(NH_2)_3]_2CO_3$). The uncoordinated water molecules and guanidinium cations are involved in an intricate hydrogen-bonding network with oxygen atoms of carboxylate groups of the ligand and the coordinated carbonate anion (Figure S10 in the Supporting Information). The Lu^{3+} ion is directly bound to seven donor atoms of the OBETA ligand, nonacoordination being completed by an η^2-carbonate ligand providing an almost symmetrical bidentate coordination (Figure 5). A similar symmetrical bidentate coordination of carbonate has been observed previously for different Ln^{3+} complexes with related ligands.[16] The five-membered chelate rings formed upon coordination of the 2,2′-oxybis(ethylamine) moiety adopt identical conformations, ($\lambda\lambda$) or ($\delta\delta$), while the chelate rings formed by the acetate arms adopt a mixed conformation, ($\delta\lambda\lambda\lambda$) or ($\lambda\delta\delta\delta$). Inspection of the crystal data shows that the $(\delta\delta)(\delta\lambda\lambda\lambda)_A$ and $(\lambda\lambda)(\lambda\delta\delta\delta)_A$ enantiomers crystallize as a racemate, where the subscript A refers to the conformations of the chelate rings formed upon coordination of the acetate groups. The different conformation adopted by the acetate containing O71 (Figure 5) nicely accommodates the relatively

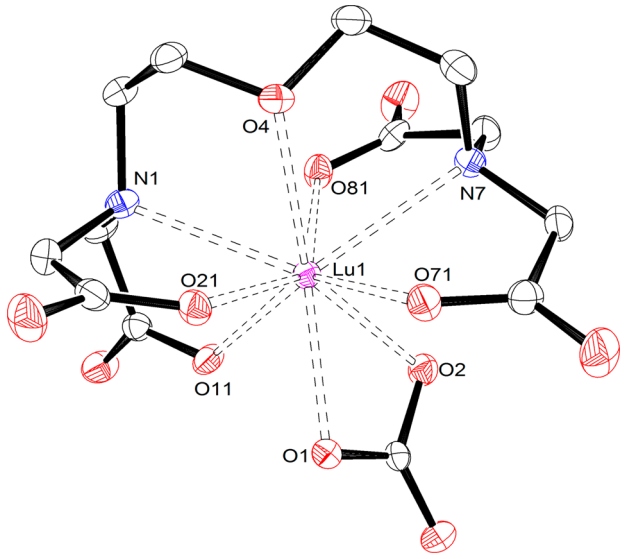

Figure 5. View of the $[Lu(OBETA)(CO_3)]^{3-}$ entity present in crystals of $[C(NH_2)_3]_3[Lu(OBETA)(CO_3)]\cdot 2H_2O$. The ORTEP plot is at the 30% probability level. Bond distances (Å): Lu1−N1 2.642(7); Lu1−N7 2.596(7); Lu1−O1 2.346(6); Lu1−O2 2.327(6); Lu1−O4 2.505(6); Lu1−O11 2.370(6); Lu1−O21 2.264(6); Lu1−O71 2.348(6); Lu1−O81 2.307(6).

bulky carbonate anion in the Lu^{3+} coordination sphere. The conformation of the ligand in $[Lu(OBETA)(CO_3)]^{3-}$ is such that two of the acetate groups are placed clearly above and below the plane defined by the three donor atoms of the 2,2′-oxybis(ethylamine) unit, while the two remaining pendant acetates are situated only slightly above (or below) that plane (those containing donor atoms O11 and O71, see Figure 5). A similar disposition of the acetate groups was previously observed for Ln^{3+} complexes containing two *N*,*N*-bis(carboxymethyl) units connected by rigid tridentate chelating units.[17]

The coordination polyhedron around the metal ion in $[Lu(OBETA)(CO_3)]^{3-}$ can be best described as a monocapped square antiprism defined by two nearly parallel pseudoplanes (Figure S11 in the Supporting Information): O4, O21, O11, and O81 define the upper plane (the mean deviation from planarity is 0.14 Å), while N7, O71, O1, and O2 define the lower plane (the mean deviation from planarity is 0.24 Å). The angle defined by these two least-squares planes is 0.8°. The amine nitrogen atom N1 caps the upper plane. The large deviation from planarity of the lower pseudoplane points to an important distortion of the coordination polyhedron. The monocapped square antiprismatic coordination in $[Lu(OBETA)(CO_3)]^{3-}$ was confirmed by performing continuous shape measurements with the assistance of the SHAPE program.[18,19] The analysis of the coordination polyhedra provides a shape measure for a spherical capped square antiprism of 1.24, while a spherical tricapped trigonal prism and a muffin give shape measures of 1.59 and 1.55, respectively (the shape measure $S(A) = 0$ for a structure fully coincident in shape with the reference polyhedron, and the maximum allowed value of $S(A)$ is 100). The coordination cage around Lu^{3+} in $[C(NH_2)_3]_3[Lu(OBETA)(CO_3)]\cdot 2H_2O$ is similar to that of $[Nd(EGTA)(H_2O)]^-$ and $[Er(EGTA)(H_2O)]^-$ complexes characterized as distorted bicapped square antiprism and distorted monocapped square antiprism geometries, respectively.[20]

dx.doi.org/10.1021/ic5020225 | *Inorg. Chem.* 2014, 53, 12499−12511

Both amine nitrogen atoms of $[Nd(EGTA)(H_2O)]^-$ are capping the upper and lower planes, whereas one of the amine nitrogen atoms in the $[Er(EGTA)(H_2O)]^-$ complex is in a capping position. The average Ln−O distances for the $[Nd(EGTA)(H_2O)]^-$ and $[Er(EGTA)(H_2O)]^-$ complexes are 2.50(3) Å and 2.36(4) Å, respectively while in the case of the Ln−N distances the average values are 2.81(1) Å and 2.57(1) Å. In the case of $[Lu(OBETA)(CO_3)]^{3-}$ the average Lu−O distance is 2.35(3) Å while the average Lu−N distance is 2.618(1). These bond lengths are significantly longer for $[Nd(EGTA)(H_2O)]^-$, while in $[Er(EGTA)(H_2O)]^-$ and $[Lu(OBETA)(CO_3)]^{3-}$ they are similar due to the similarity in coordination environments and ionic radii of Er^{3+} and Lu^{3+} ions. However, the angles defined by the two least-squares planes of $[Nd(EGTA)(H_2O)]^-$ and $[Er(EGTA)(H_2O)]^-$ complexes are 26° and 23°, which are significantly larger than that of $[Lu(OBETA)(CO_3)]^{3-}$ due to the longer ligand backbone of EGTA.

Solution Structure and Dynamics. To obtain information on the solution structure and dynamics of the $[Gd(OBETA)(H_2O)_2]^-$ complex we have investigated the ^1H NMR spectra of the diamagnetic Y^{3+} analogue at different temperatures. The ^1H NMR spectrum of Y(OBETA) obtained at 298 K (Figure 6) shows two signals at 2.63 and 3.53 ppm

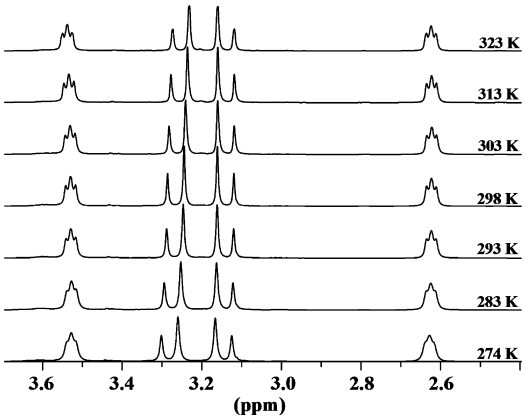

Figure 6. 400 MHz ^1H NMR spectra of Y(OBETA) complex recorded at different temperatures ([YL] = 0.1 M, pH = 7.0, D_2O).

due to the protons of the $N-CH_2-CH_2-O$ units. Furthermore, the protons of the acetate groups provide an AB spin system at 3.15 and 3.28 ppm with ^2J = 16.6 Hz at 274 K. A close inspection of the ^1H NMR spectra reported in Figure 6 reveals that there is an increase in the $\Delta\delta$ of signals due to the AB spin system and the triplet at. 3.53 ppm as the temperature is increased. This points to the presence of dynamic exchange processes in solution, which are fast on the NMR time scale. Assuming that the conformation of the complex in solution is similar to that observed in the solid state for $[Lu(OBETA)(CO_3)]^{3-}$, the ^1H NMR spectra are consistent with the presence in solution of a dynamic process that exchanges (i) the geminal protons of the 2,2′-oxybis(ethylamine) units and (ii) the in-plane and out-of-plane acetate groups. The AB spin system observed for the protons of the acetate arms indicates that the methylene protons of the interchanging acetate groups remain nonequivalent throughout this process. This indicates that isomer interconversion does not require dissociation of the acetate groups. The ^1H NMR spectrum of the paramagnetic Eu^{3+} analogue (Figure S12 in the Supporting Information) shows four signals at 15.4, 2.3, −10.1, and −11.4 ppm, in agreement with these observations.

As described previously on related complexes,[21] the coordination of OBETA to the Ln^{3+} ion implies the occurrence of two helicities: one associated with the layout of the acetate arms (absolute configuration Δ or Λ), and the other with the two five-membered chelate rings formed by the binding of the $O-CH_2-CH_2-N$ moieties (each of them showing absolute configuration δ or λ).[22] Furthermore, the four five-membered chelate rings formed upon coordination of the acetate groups can adopt δ or λ conformations as well. However, an overall Δ chirality of the complex imposes δ conformations for the four five-membered rings formed upon binding of the carboxylate functions, while an overall Λ chirality results in λ conformations. A careful investigation of the conformational space of the $[Gd(OBETA)(H_2O)_2]^-$ system using DFT calculations provides the minimum energy conformation shown in Figure 7. According to our calculations, the four

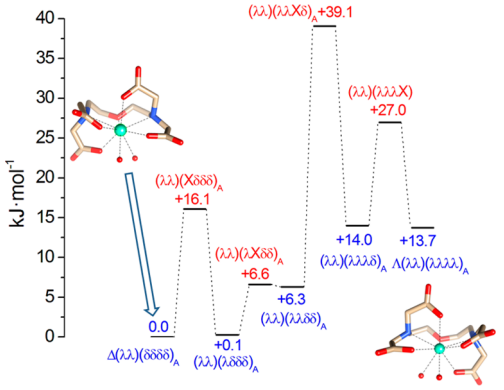

Figure 7. Relative free energies of minima, intermediates, and transition states (TSs) involved in the $\Delta(\lambda\lambda)(\delta\delta\delta\delta)_A \rightarrow \Lambda(\lambda\lambda)(\lambda\lambda\lambda\lambda)_A$ interconversion process of $[Gd(OBETA)(H_2O)_2]^-$ in aqueous solution.

five-membered chelate rings formed upon coordination of the acetate groups adopt identical δ conformations. Furthermore, the two five-membered chelate rings formed by the binding of the $O-CH_2-CH_2-N$ moieties adopt δ conformations, which results in an overall $\Delta(\lambda\lambda)(\delta\delta\delta\delta)_A$ conformation of the complex. Thus, according to our calculations, $[Gd(OBETA)(H_2O)_2]^-$ exists in solution as the $\Delta(\lambda\lambda)(\delta\delta\delta\delta)_A/\Lambda(\delta\delta)(\lambda\lambda\lambda\lambda)_A$ enantiomeric pair. However, it should be noted that the asymmetrical $(\lambda\lambda)(\lambda\delta\delta\delta)_A$ conformation observed in the solid state for the Lu^{3+} complex is only 0.1 kJ·mol^{-1} less stable than the symmetrical $(\lambda\lambda)(\delta\delta\delta\delta)_A$ form of $[Gd(OBETA)(H_2O)_2]^-$ (Figure 7). This energy difference is clearly within the error margin of the computational method, and it is likely that both conformations are present in significant populations in aqueous solution. However, the interconversion between these two forms does not explain the observed NMR spectra, which indicate exchange between the in-plane and out-of-plane acetate groups. Assuming that the complex exists in solution as the $\Delta(\lambda\lambda)(\delta\delta\delta\delta)_A/\Lambda(\delta\delta)(\lambda\lambda\lambda\lambda)_A$ enantiomeric pair, the ^1H NMR spectra are consistent with the presence of a fast $\Delta(\lambda\lambda)(\delta\delta\delta\delta)_A \leftrightarrow \Lambda(\delta\delta)(\lambda\lambda\lambda\lambda)_A$ (or $(\lambda\lambda)(\lambda\delta\delta\delta)_A \leftrightarrow (\delta\delta)(\delta\lambda\lambda\lambda)_A$) enantiomerization process in solution.

DFT calculations performed on the La^{3+} and Lu^{3+} complexes ($\Delta(\lambda\lambda)(\delta\delta\delta\delta)_A$ isomer) show that the bond lengths between the metal ion and the donor atoms of the ligand decrease along

dx.doi.org/10.1021/ic5020225 | Inorg. Chem. 2014, 53, 12499−12511

the lanthanide series (Table S1 in the Supporting Information), as is usually observed for Ln^{3+} complexes as a consequence of the lanthanide contraction.[23] The Ln−O and Ln−N bond distances are close to those observed in nine-coordinate Ln^{3+} complexes with polyaminopolycarboxylate ligands.[4] The Gd−O distances to oxygen atoms of the coordinated water molecules (2.58 and 2.62 Å) are ca. 0.1 Å longer than that normally assumed in the analysis of ^{17}O NMR longitudinal relaxation data of nine-coordinate Gd^{3+} complexes (2.50 Å). This effect is attributed to the fact that continuum models of solvation cannot account for specific solvent−solute interactions such as hydrogen-bonding interactions between inner-sphere and second-sphere water molecules.[24]

A more detailed picture of the dynamics of the $[Gd(OBETA)(H_2O)_2]^-$ complex was obtained using DFT calculations in aqueous solution. According to our results obtained on B3LYP/6-31G(d) optimized geometries in aqueous solution, the Δ ↔ Λ interconversion involves the rotation of the acetate groups of the ligand that exchange the in-plane and out-of-plane carboxylate units. Our DFT calculations performed on the $\Delta(\lambda\lambda)(\delta\delta\delta\delta)_A$ form of the $[Gd(OBETA)(H_2O)_2]^-$ system show that the Δ ↔ Λ interconversion is a four step process involving the stepwise rotation of each of the acetate groups of the ligand (Figure 7). Each of these rotation processes results in the inversion of one of the five-membered chelate rings formed upon coordination of the acetate groups, which changes its configuration from λ to δ. The stepwise inversion of these four chelate rings results in the formation of the $\Lambda(\lambda\lambda)(\lambda\lambda\lambda\lambda)_A$ isomer. Assuming that the rate-determining step for the Δ ↔ Λ interconversion corresponds to the transition state with the highest energy (Figure 7), the barrier for this process amounts to 39.1 kJ·mol^{-1}. This activation barrier is much lower than that determined experimentally and computationally for the acetate rotation process in Ln^{3+} DOTA complexes.[25a−c]

The inversion of each of the five-membered chelate rings formed upon coordination of the 2,2′-oxybis(ethylamine) moiety of the ligand involves a TS in which the ring adopts a nearly planar conformation with the OCCN moiety in eclipsed disposition (Figure 8). Previous HF[26] and DFT[25] calculations performed on Ln^{3+} complexes of ligands derived from 1,4,7,10-tetraazacyclododecane provided similar TSs for the inversion of the five-membered chelate rings formed upon coordination of the ethylenediamine units. The activation free energies calculated for the inversion of the chelate rings (Figure 7) fall within the range 25−44 kJ·mol^{-1}. These values are considerably lower than those determined experimentally for the inversion of ethylenediamine units in Ln^{3+} polyaminopolycarboxylate complexes such as $[Ln(DTPA)(H_2O)]^{2-}$, [Nd(DTPA-BPA)], and $[Yb(DOTA)]^-$, which are in the range 50−65 kJ·mol^{-1}.[27]

Noteworthy is that the activation free energies calculated for the rotation of the acetate groups and the inversion of the chelate rings formed upon coordination of the 2,2′-oxybis(ethylamine) unit in $[Gd(OBETA)(H_2O)_2]^-$ are very similar. Our calculations predict a rather low activation free energy for the $\Delta(\lambda\lambda)(\delta\delta\delta\delta)_A \leftrightarrow \Lambda(\delta\delta)(\lambda\lambda\lambda\lambda)_A$ racemization process (ca. 40 kJ·mol^{-1}), in agreement with the behavior of the complexes in solution. Thus, $[Ln(OBETA)(H_2O)_2]^-$ possesses a very flexible metal coordination environment, which is also responsible for the relatively fast water exchange of the inner-sphere water molecule observed for the Gd^{3+} analogue (see below).[28]

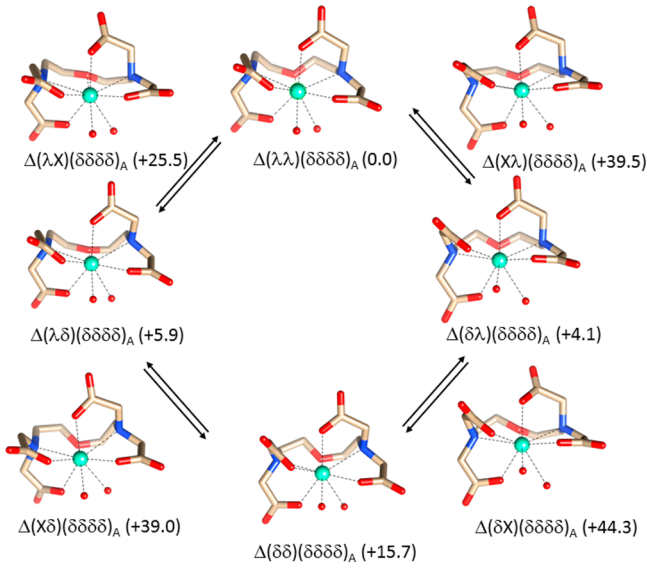

Figure 8. Minimum energy conformations obtained from DFT calculations (B3LYP) in aqueous solution for $[Gd(OBETA)(H_2O)_2]^-$ and relative free energies (kJ·mol^{-1}) of minima, intermediates, and transition states (TSs) involved in the $\Delta(\lambda\lambda)(\delta\delta\delta\delta)_A \rightarrow \Delta(\delta\delta)(\delta\delta\delta\delta)_A$ interconversion process of $[Gd(OBETA)(H_2O)_2]^-$ in aqueous solution. A nearly planar conformation with the OCCN moiety in eclipsed disposition is denoted as X. Hydrogen atoms are omitted for simplicity.

In spite of the rather flexible structure of Ln(OBETA) complexes evidenced by NMR experiments and DFT calculations, Ln(EGTA) complexes appear to be even more flexible. In fact, the structural behavior of several Ln(EGTA) complexes was studied in detail earlier, showing fast rearrangement of Ln(EGTA) complexes at room temperature.[29] To get more insight, a variable temperature ^1H NMR study on Y(EGTA) (Figure S13 in the Supporting Information) was undertaken and compared to analogous experiments carried out on Y(OBETA) (Figure 7). At low temperatures the signals of the acetate methylene protons of Y(EGTA) are observed as an AB multiplet at 3.18 ppm, which broadens and coalesces at higher temperatures as a result of an increased rate in the isomerization processes. The exchange between the acetate methylene protons implies the inversion of the amine nitrogen atoms of the ligand, and requires the partial dissociation of at least one acetate group. However, the AB multiplet of the acetate methylene protons of Y(OBETA) is unchanged in the temperature range 274−323 K, clearly indicating a less flexible structure of Y(OBETA) with respect to Y(EGTA).

NMR Relaxometric Study. The relaxivity value (r_1, i.e., the increase in the nuclear magnetic relaxation rate of the water protons normalized to a 1 mM aqueous solution of the Gd^{3+} complex) reported for $[Gd(OBETA)(H_2O)_2]^-$ (ref 8 and Table 4) is consistent with the presence of two water molecules in the inner coordination sphere of the metal ion ($q = 2$), as it is close to the values measured in analogous conditions for other $q = 2$ Gd^{3+} complexes of comparable molecular weight. The value of the hydration number was also confirmed by luminescence lifetime measurements on the related Eu^{3+} complex.[8,30] As r_1 depends on the magnetic field strength, temperature, and several important molecular parameters of the paramagnetic metal complex that describe the magnetic coupling between the solvent nuclei and Gd^{3+}, a complete ^1H and ^{17}O NMR relaxometric study was carried out to obtain

dx.doi.org/10.1021/ic5020225 | Inorg. Chem. 2014, 53, 12499−12511

Table 4. Parameters Obtained from the Simultaneous Analysis of ^{1}H NMRD Profiles and ^{17}O NMR Data (11.75 T) for the Gd^{3+} Complexes of OBETA and Related Ligands (DO3A (1,4,7,10-Tetraazacyclododecane-1,4,7-triacetic Acid),[6a] TREN-bis(6-Me-HOPO)(TAM-TRI),[6b] PTDITA,[6c] and AAZTA[5])[a]

params	Gd(OBETA)	Gd(EGTA)[b]	Gd(DO3A)[c]	Gd[TREN-bis(6-Me-HOPO)(TAM-TRI)][d]	Gd(PTDITA)[e]	Gd(AAZTA)[f]
$^{20}r_1^{298}$ (mM^{-1} s^{-1})	7.2	4.6	6.0	8.9	10.2	7.1
Δ^2 (10^{19} s^{-2})	4.3 ± 0.1	3.4	4.6	8.7	2.5	2.2
τ_V^{298} (ps)	17 ± 2	24	14	24	2	31
k_{ex}^{298} (10^6 s^{-1})	13 ± 1	31	6.4	52.6	3.3	11.1
τ_R^{298} (ps)	65 ± 4	58	66	118	105	74
q	2[g]	1[g]	1.9	2	2[g]	2
r (Å)	3.00[g]	3.00[g]	3.15	3.10	3.00[g]	3.10
E_V (kJ/mol)	1.0[g]	1.0[g]	2.0	2.0	1.0[g]	
$\Delta H^{\ddagger}_M$ (kJ/mol)	40.1 ± 2.3	42.7	44	25.9	37.7	
$A_O/\hbar$ (10^6 rad/s)	−2.9 ± 0.2	−3.2	−3.8	−3.8	−3.3	−3.8

[a]See Figure 1 for the chemical structures. [b]Reference 29. [c]Reference 6a. [d]Reference 6b. [e]Reference 6c. [f]Reference 5. [g]Values fixed in the fitting.

detailed information on the physicochemical characteristics of $[Gd(OBETA)(H_2O)_2]^-$.

The variation of r_1 as a function of the magnetic field strength, the so-called nuclear magnetic resonance dispersion profile (^{1}H NMRD), was measured at 283, 298, and 310 K in the proton Larmor frequency range 0.01−70 MHz, corresponding to magnetic field strengths varying between 2.34×10^{-4} and 1.64 T (Figure 9). The profiles show the characteristic features

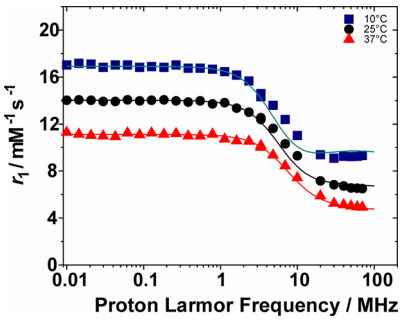

Figure 9. $1/T_1$ ^{1}H NMRD profiles for $[Gd(OBETA)(H_2O)_2]^-$ at pH = 7.0 and 283 K (blue squares); 298 K (black circles); 310 K (red triangles). The solid lines represent the results of the best-fitting to the experimental data (see Table 4).

of low molecular weight complexes, i.e.: a plateau at low fields, a dispersion around 4−8 MHz, and another plateau with lower relaxivity in the high-frequency region (>20 MHz). This behavior is quite typical for Gd chelates whose relaxivity is largely dominated by rotational dynamics. The temperature dependence of r_1 for $[Gd(OBETA)(H_2O)_2]^-$ showed an exponential increase with decreasing temperature and thus the typical behavior of systems in the fast-exchange regime.[8] More accurate and quantitative information on the kinetics of the water exchange could be obtained by measuring the temperature dependence of the solvent ^{17}O NMR transverse relaxation rates, R_2, and shifts, $\Delta\omega$, at 11.75 T on a 7 mM solution of the complex at neutral pH.

The reduced transverse relaxation rates ($1/T_{2r}$) increase with decreasing temperature with a maximum at about 290 K (Figure 10). This is clearly indicative of a rate of water exchange much faster than that measured for the commercial CAs $[Gd(DTPA)]^{2-}$ and $[Gd(DOTA)]^-$ for which the curve shows a maximum shifted at higher temperature (ca. 315 K).[31] The experimental data, ^{1}H NMRD and ^{17}O NMR, were fitted simultaneously, according to the established theory of paramagnetic relaxation expressed in terms of the Solomon−Bløembergen−Morgan[32] and Freed[33] equations for the inner-sphere (IS) and outer-sphere (OS) proton relaxation mechanisms, respectively, and of the Swift−Connick theory for ^{17}O relaxation.[34] The IS contribution to r_1 is determined by the number of bound water molecules and their rate of exchange ($k_{ex} = 1/\tau_M$), the molecular rotational correlation time (τ_R), and the electronic relaxation times ($T_{1,2e}$) of Gd^{3+}. The OS term depends on $T_{1,2e}$, the relative diffusion coefficient between the complex and the water molecules (D), and their distance of closest approach, a.

The ^{17}O R_2 data depend primarily on $T_{1,2e}$, the hyperfine $Gd-^{17}O_{water}$ coupling constant $A_O/\hbar$, τ_M, and q. Information on q and $A_O/\hbar$ are derived from the temperature dependence of $\Delta\omega$. Additional relevant parameters are those associated with the electronic relaxation times $T_{1,2e}$, i.e., the trace of the square

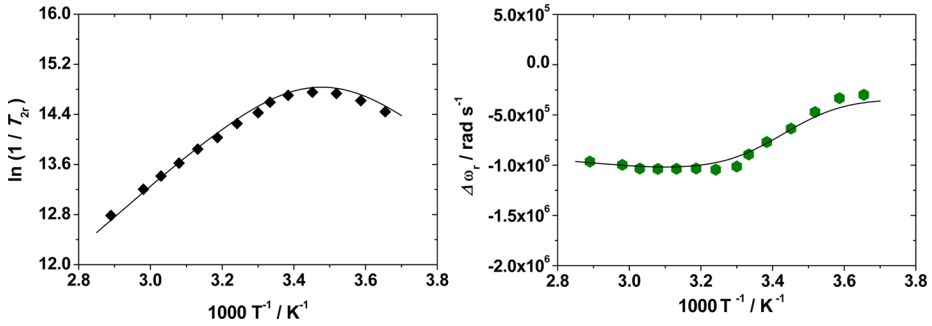

Figure 10. Temperature dependence of the reduced water ^{17}O NMR transverse relaxation rates (left) and chemical shifts (right) at 11.75 T and pH = 7 for a 7 mM solution of Gd(OBETA).

dx.doi.org/10.1021/ic5020225 | Inorg. Chem. 2014, 53, 12499−12511

of the zero-field splitting tensor, Δ^2; the correlation time describing the modulation of the zero-field splitting, τ_V, and its activation energy, E_V; the enthalpy of activation, $\Delta H_M^{\ddagger}$, for the water exchange process.

A reasonable estimate of some of the relaxation parameters is typically done during the fitting: q was fixed to 2; the distance between the metal ion and the protons of the bound water molecule, r, was fixed to 3.0 Å; a was fixed to 4 Å and D to 1.6, 2.24, and 3.1 × 10^{-5} cm^2 s^{-1} at 283, 298, and 310 K, respectively. These values are typical for small Gd^{3+} chelates, which provide diffusion coefficients very similar to those of water in pure water (D^{298} = 2.3 × 10^{-5} cm^2 s^{-1} and E_D = 17.3 kJ·mol^{-1}).[35] The typical values of 1.0 and 16 kJ·mol^{-1} were assigned to the activation energy for the modulation of the zero-field splitting interaction (E_V) and to the rotational motion of the complex (E_R). The relevant best-fit parameters are listed in Table 4 and compared with those of related q = 2 Gd^{3+} complexes of similar size.

The rotational correlation time τ_R is quite comparable to those calculated for Gd(AAZTA) and Gd(EGTA) while the longer values of Gd[TREN-bis(6-Me-HOPO)(TAM-TRI)] and Gd(PTDITA) simply reflect their higher molecular weight (AAZTA, 6-amino-6-methylperhydro-1,4-diazepine-*N*,*N*′,*N*″,*N*″-tetraacetic acid; TREN-bis(6-Me-HOPO)(TAM-TRI), tris(2-aminoethyl)amine-bis(6-methyl-3-hydroxy-2-pyridinone)(terephthalamide-triethylene glycol-monoethyl ether); PTDITA, 2,2′,2″,2‴-[(6-piperidinyl-1,3,5-triazine-2,4-diyl)dihydrazin-2-yl-1-ylidene]tetraacetic acid). The parameters associated with the electronic relaxation, Δ^2 and τ_V, show values for Gd(OBETA) in agreement with those found for Gd-(EGTA) and for the other bis-aquo Gd^{3+} complexes. Only for Gd[TREN-bis(6-Me-HOPO)(TAM-TRI)] the value of Δ^2 is ca. 3 times longer, suggesting a less symmetric instantaneous structure and a faster electronic relaxation. The values of k_{ex} vary more markedly between the different complexes as a consequence of the differences in the structural characteristics. For Gd(OBETA) the rate of water exchange appears to be quite similar to that of Gd(AAZTA) (same charge) but much greater than that of Gd(PTDITA). On the other hand, the value of k_{ex} is about half compared to that measured for the congener complex Gd(EGTA). In this latter case, such a high rate of exchange was attributed to a destabilizing effect of the bound water caused by steric interaction with the 1,2-ethylenedioxy bridge. Conceivably, the lack of this structural group in OBETA diminishes the steric compression and stabilizes the coordinated water molecules in the Gd^{3+} chelate. The case of the HOPO derivative is different in that the very high k_{ex} value is associated with the presence of an eight-coordinate Gd^{3+} ion, and then with a water exchange mechanism associatively activated.

The scalar coupling constant, $A_O/\hbar$, assumes a value only slightly lower than for other complexes. This difference is not very significant and could reflect minor variations in the r_{GdO} distance value that we fixed to 3.00 Å for Gd(OBETA).

In a preliminary study, we observed that Gd(OBETA) has only a very weak tendency to form ternary complexes at neutral pH in the presence of a 20-fold molar excess of bidentate oxoanions of biological relevance such as lactate, citrate, and phosphate.[8] In addition, the invariant r_1 value also at high pH (pH = 10) showed that carbonate anions dissolved in the aerated aqueous solution do not coordinate Gd^{3+} replacing the bound water molecules.[8] However, at pH ∼ 9.5, the formation of $[Gd(OBETA)(CO_3)]^{3-}$ can occur as shown by measuring the change of the relaxation rate for a 1 mM Gd(OBETA) solution as a function of increasing concentration of CO_3^{2-} ions (Figure S14 in the Supporting Information). From this experiment, a value of 2.60(2) could be determined for the stability constant, log $K_{Gd(L)CO_3}$, of the $[Gd(OBETA)(CO_3)]^{3-}$ ternary complex. This agrees well with the corresponding value of 2.0(1) calculated from kinetic data. Moreover, the calculated r_1 value of 2.7(1) mM^{-1} s^{-1} indicates that CO_3^{2-} coordinates in a bidentate manner to the Gd^{3+} ion by displacing both inner-sphere water molecules.

CONCLUSIONS

The results of a comprehensive investigation including solution thermodynamic, kinetic, X-ray diffractometry, ^{1}H NMR, molecular modeling, and relaxometric studies have elucidated the reasons underlying the unexpected higher stability of Ln(III) complexes of the heptadentate ligand OBETA as compared to the octadentate congener EGTA. The structural study reveals a different arrangement of the donor atoms in the coordination polyhedron around the metal center. As a result, Ln(OBETA) complexes show a significantly higher conformational and coordination rigidity, confirmed by VT-^{1}H NMR spectra for the diamagnetic Y(OBETA) chelate. The stability trend previously observed along the lanthanide series, with a peak around Gd, is confirmed as well as the values of log $K_{Ln(OBETA)}$ being greater than those of EGTA, with the exception of the late members (Yb and Lu). The thermodynamic behavior is closely paralleled by the superior inertness of Ln(OBETA) chelates, whose dissociation proceeds by the general acid catalyzed pathway, and that involves the conjugate acids of biologically relevant anionic species such as phosphate and carbonate for the protonation step and the formation of ternary Ln(OBETA)X complexes. The formation of the latter is further confirmed by the diffractometric analysis performed on $[C(NH_2)_3]_3[Lu(OBETA)(CO_3)]\cdot 2H_2O$, where carbonate is involved in an η^2-coordination mode. Finally, the relaxometric studies on Gd(OBETA) confirm an enhanced relaxivity value associated with the presence of two coordinated water molecules in a fast-exchange regime. The r_1 value is stable over a wide range of pH, being affected only in significantly basic environments with high concentration of bidentate anions. The uncommon combination of these favorable properties prompts us to continue the investigation of this chelator and suitably modified derivatives for the development of improved Ln(III)-based imaging probes.

EXPERIMENTAL SECTION

Materials. The chemicals used for the experiments were of analytical grade. The concentrations of the $MgCl_2$, $CaCl_2$, $MnCl_2$, $ZnCl_2$, $CuCl_2$, and $LnCl_3$ solutions were determined by complexometric titration with standardized Na_2H_2EDTA and Xylenol Orange ($ZnCl_2$, and $LnCl_3$), Murexide ($CuCl_2$), Patton & Reeder's ($CaCl_2$), and Eriochrome Black T ($MgCl_2$, $MnCl_2$) as indicators. The concentrations of the stock solutions of H_4OBETA[8] and H_4EGTA (Fluka) were determined by pH potentiometric titration in the presence and absence of a large (40-fold) excess of $CaCl_2$. The pH potentiometric titrations were carried out with standardized 0.2 M KOH.

Equilibrium Measurements. The stability and protonation constants of Mg^{2+}, Ca^{2+}, Mn^{2+}, Zn^{2+}, Cu^{2+}, and Ln^{3+} complexes formed with OBETA and EGTA ligands were determined by pH potentiometric titration. The metal-to-ligand concentration ratio was 1:1, but for the Cu^{2+} and Zn^{2+} complexes titrations were also made at a metal-to-ligand ratio of 2:1 (the concentration of the ligand was

generally 0.002 M). For the pH measurements and titrations, a Metrohm 785 DMP Titrino titration workstation and a Metrohm-6.0233.100 combined electrode were used. Equilibrium measurements were carried out at a constant ionic strength (0.1 M KCl) in 6 mL samples at 25 °C. The solutions were stirred under N_2 atmosphere. The titrations were made in the pH range of 1.7−11.7. KH-phthalate (pH = 4.005) and borax (pH = 9.177) buffers were used to calibrate the pH-meter. For the calculation of $[H^+]$ from the measured pH values, the method proposed by Irving et al. was used.[36] A 0.01 M HCl solution was titrated with the standardized KOH solution in the presence of 0.1 M KCl ionic strength. The differences between the measured (pH_{read}) and calculated pH ($-\log [H^+]$) values were used to obtain the equilibrium H^+ concentration from the pH values, measured in the titration experiments.

The stability constants of the Cu(OBETA) complex were determined by spectrophotometry by studying the absorption band of Cu^{2+} complexes at $[H^+]$ = 0.01−0.42 M in the wavelength range 400−800 nm. The concentrations of Cu^{2+} and OBETA were 1.5 mM. The H^+ concentration in the samples was adjusted with the addition of calculated amounts of 3.00 M HCl. The samples were kept at 25 °C for a week. The absorbance values of the samples were determined at 11 wavelengths (575, 595, 615, 635, 655, 675, 695, 715, 735, 755, and 775 nm). For the calculations of the stability and protonation constants of Cu(OBETA), the molar absorptivities of $CuCl_2$, Cu(OBETA), Cu(HOBETA), Cu(H_2OBETA), Cu_2(OBETA), and Cu_2(OBETA)H_{-1} were determined by recording the spectra of 2.0×10^{-3}, 4.0×10^{-3} and 6.0×10^{-3} M solutions of $CuCl_2$, Cu(OBETA), and Cu_2(OBETA) in the pH range 1.7−6.0. The pH was adjusted by stepwise addition of concentrated aqueous KOH or HCl. The spectrophotometric experiments were performed with a Cary 1E spectrophotometer in a 1 cm quartz cuvette at 25 °C. The protonation and stability constants were calculated with the PSEQUAD program.[37]

Kinetic Studies. The rates of dissociation of the Gd(OBETA) and Gd(EGTA) complexes were studied by spectrophotometry, with the use of the metal exchange (transmetalation) reactions occurring between the complexes and Cu^{2+} in the presence of citrate excess. The effect of the presence of $KHCO_3$ and KH_2PO_4/K_2HPO_4 on the rate of reactions was also investigated. The formation of the Cu^{2+}−polyaminopolycarboxylate complexes was followed with a Cary 1E spectrophotometer at 300 nm and 25 °C. A 0.1 M KCl concentration was used to keep the ionic strength constant. In order to keep the pH values constant, MES (pH range of 6.0−6.5), HEPES (pH range of 7.0−8.0), and 1,4-dimethylpiperazine (pH range of 8.0−9.5) buffers were used in 0.01 M concentration.

NMR Measurements. ^{1}H NMR spectra of OBETA, Y(OBETA), and Y(EGTA) were recorded by using a Bruker DRX 400 (9.4 T) NMR spectrometer equipped with a Bruker VT-1000 thermocontroller and a BB inverse *z* gradient probe (5 mm). The protonation process of the H_4OBETA ligand was followed by ^{1}H NMR spectroscopy. A 0.01 M solution of the ligand in H_2O with 5% D_2O was prepared for these experiments. The pH was adjusted by stepwise addition of KOH and/or HCl (both prepared in H_2O). The calculations were performed by using the computer program Micromath Scientist, version 2.0 (Salt Lake City, UT, USA). ^{1}H NMR spectra of Y(OBETA) and Y(EGTA) were recorded by using 0.1 M solutions of the Y^{3+} complexes (both Y^{3+} complexes were prepared in D_2O). The chemical shifts are reported in ppm, using DSS (4,4-dimethyl-4-silapentane-1-sulfonic acid) as an internal standard. The spectra were analyzed with the Bruker WinNMR software package.

Computational Details. All calculations were performed employing hybrid DFT with the B3LYP exchange-correlation functional,[38] and the Gaussian 09 package (Revision A.02).[39] Full geometry optimizations of the $[Ln(OBETA)(H_2O)_2]^-$ systems (Ln = La, Gd or Lu) were performed in aqueous solution by using the large-core (LC) effective core potential (ECP) of Dolg et al. and the related [5s4p3d]-GTO valence basis set for the lanthanides,[40] and the 6-31G(d) basis set for C, H, N, and O atoms. This ECP includes 46 + $4f^n$ electrons in the core, leaving the outermost 11 electrons to be treated explicitly. The use of large core ECPs has been justified by the fact that 4f orbitals do not significantly contribute to bonding due to their limited radial extension as compared to the 5d and 6s shells.[41] The use of large-core ECPs avoids many difficulties associated with the computational treatment of open-shell systems, and despite their approximate nature they are an efficient computational tool that has proven to give good results in studies that focus on the structural features or the estimates of relative energies for Ln(III) complexes at both the HF and DFT levels.[42] No symmetry constraints have been imposed during the optimizations. The default values for the integration grid ("fine") and the SCF energy convergence criteria (10^{-8}) were used. The stationary points found on the potential energy surfaces as a result of the geometry optimizations have been tested to represent energy minima rather than saddle points via frequency analysis. Solvent effects were evaluated by using the polarizable continuum model (PCM), in which the solute cavity is built as an envelope of spheres centered on atoms or atomic groups with appropriate radii. In particular, we used the integral equation formalism (IEFPCM) variant as implemented in Gaussian 09.[43] The relative free energies of the different conformations of $[Gd(OBETA)(H_2O)_2]^-$ were calculated in aqueous solution at the B3LYP/6-31G(d) level, including non-potential-energy contributions (zero point energies and thermal terms) obtained through frequency analysis. The interconversion between different isomers was investigated by means of the synchronous transit-guided quasi-Newton method.[44] The nature of the saddle points and intermediates was characterized by frequency analysis. The free energy barriers include non-potential energy contributions (that is, zero point energies and thermal terms) obtained by frequency analysis.

X-ray Diffraction Experiments. Single crystal X-ray diffraction data were collected at 293 (1) K with an Enraf Nonius MACH3 diffractometer, Mo Kα radiation λ = 0.71073 Å, ω motion. Raw data were evaluated using the XCAD4 software;[45] the structure was solved using direct methods[46] and refined on F^2 using the SHELX-97 program.[47] The Platon package[48] was used for crystallographic calculations, while publication material was prepared with the WINGX-97 suite.[49] Colorless block (0.35 × 0.25 × 0.1 mm) crystals of $C_{16}H_{38}LuN_{11}O_{14}$, M = 783.54, monoclinic, a = 9.4880(18) Å, b = 14.232(5) Å, c = 20.620(5) Å, β = 93.60(5)°, V = 2779(1) Å^3, Z = 4, space group: $P21/n$ (No. 14), ρ_{calc} = 1.873 g cm^{-3}. θ_{max} = 26.0°, 6259 measured reflections of which 5451 were independent and 4925 were unique with $I > 2\sigma(I)$; decay: 0%, $R(F)$ = 0.057 and $wR(F^2)$ = 0.148 for 5451 reflections, 391 parameters, 6 restraints. Residual electron density: 3.46/−3.70 e/Å^3 close to the lutetium atom. Heavy atoms were refined anisotropically. Hydrogen atoms were treated with a mixture of independent and constrained refinement. The difference electron density map shows the position of the guanidine protons and in some cases water protons. Water molecules can be in various orientations in the lattice, and therefore the description of the hydrogen bond pattern is ambiguous.

Relaxometric Measurements. The water−proton longitudinal relaxation rates as a function of the magnetic-field strength were measured in nondeuterated aqueous solutions on a fast field-cycling Stelar SmarTracer relaxometer (Stelar s.r.l., Mede (PV), Italy) over a continuum of magnetic-field strengths from 0.00024 to 0.25 T (corresponding to 0.01−10 MHz proton Larmor frequencies). The relaxometer operates under computer control with an absolute uncertainty in $1/T_1$ of ±1%. Additional longitudinal and transverse relaxation data in the range 15−70 MHz were obtained on a Stelar Relaxometer connected to a Bruker WP80 NMR electromagnet adapted to variable-field measurements. The exact concentration of Gd^{3+} ions was determined by measurement of the bulk magnetic-susceptibility shifts of a *t*BuOH signal. The ^{1}H T_1 relaxation times were acquired by the standard inversion−recovery method with a typical pulse width (90°) of 3.5 ms and 16 experiments of 4 scans. The temperature was controlled with a Stelar VTC-91 airflow heater equipped with a calibrated copper−constantan thermocouple (uncertainty of ±0.1 °C). Variable-temperature ^{17}O NMR measurements were recorded on a Bruker Avance III spectrometer (11.74 T, 67.8 MHz for ^{17}O) equipped with a 5 mm probe and standard temperature control units. An aqueous solution of the complex containing 1.0% of the ^{17}O isotope (Cambridge Isotope) was used. The observed

dx.doi.org/10.1021/ic5020225 | Inorg. Chem. 2014, 53, 12499−12511

transverse relaxation rates were calculated from the signal width at half-height.

■ ASSOCIATED CONTENT

Supporting Information

^{1}H NMR studies of the protonation process of OBETA. Equations used for the evaluation of the complexation equilibria for OBETA and EGTA. Definitions and equations used for the evaluation of the dissociation kinetics of Gd(OBETA) and Gd(EGTA) in the presence of endogenous ligands. Packing diagram and coordination polyhedron for $[C(NH_2)_3]_3[Lu(OBETA)(CO_3)]\cdot 2H_2O$. ^{1}H NMR spectra of Eu(OBETA) and Y(EGTA). Crystallographic data in cif format. This material is available free of charge via the Internet at http://pubs.acs.org.

■ AUTHOR INFORMATION

Corresponding Authors

*E-mail: mauro.botta@unipmn.it.

*E-mail: giovenzana@pharm.unipmn.it.

Present Address

#J.B.: MTA-PE Research Group for Translational Glycomics, University of Pannonia, H-8200 Veszprém, Egyetem utca 10, Hungary.

Notes

The authors declare no competing financial interest.

■ ACKNOWLEDGMENTS

This research was supported by the Compagnia di San Paolo (CSP-2012 NANOPROGLY Project) (R.N., L.T., M.B., G.B.G.), by the European Union and the State of Hungary, cofinanced by the European Social Fund in the framework of TÁMOP 4.2.4. A/2-11-1-2012-0001 "National Excellence Program" (Grant No. A2-MZPD-12-0038) (Z.B). The authors also thank the Hungarian Scientific Research Found (OTKA K109029 and K84291) and ENVIKUT project (Grant No. TÁMOP-4.2.2.A-11/1/KONV-2012-0043) implemented through the New Hungary Development Plan, cofinanced by the European Social Fund and the European Regional Development Fund for financial support (A.C.B., J.B., A.V.). The Italy-Hungary Intergovernmental S&T Cooperation Program (HU11MO2-TET_10-1-2011-0202) is also gratefully acknowledged. C.P.-I. thanks Centro de Supercomputación de Galicia (CESGA) for providing the computer facilities. This study was performed under the auspices of EU-COST Action TD1004.

■ REFERENCES

(1) Brown, M. A.; Semelka, R. P. *MRI—Basic Principles and Application*; John Wiley & Sons: Hoboken, NJ, USA, 2003.

(2) Merbach, A. S.; Helm, L.; Toth, E. *The Chemistry of Contrast Agents in Medical Magnetic Resonance Imaging*, 2nd ed.; John Wiley and Sons: Chichester, U.K., 2013.

(3) (a) Gielen, M.; Tiekink, E. R. *Metallotherapeutic Drugs and Metal-Based Diagnostic Agents*; WILEY: Chichester, 2005. (b) Reichert, D. E.; Lewis, J. S.; Anderson, C. R. *Coord. Chem. Rev.* **1999**, *184*, 3−66.

(4) Caravan, P.; Ellison, J. J.; McMurry, T. J.; Lauffer, R. B. *Chem. Rev.* **1999**, *99*, 2293−2352.

(5) (a) Aime, S.; Calabi, L.; Cavallotti, C.; Gianolio, E.; Giovenzana, G. B.; Losi, P.; Maiocchi, A.; Palmisano, G.; Sisti, M. *Inorg. Chem.* **2004**, *43*, 7588−7590. (b) Baranyai, Z.; Uggeri, F.; Giovenzana, G. B.; Bényei, A.; Brücher, E.; Aime, S. *Chem.—Eur. J.* **2009**, *15*, 1696−1705. (c) Gugliotta, G.; Botta, M.; Tei, L. *Org. Biomol. Chem.* **2010**, *8*, 4569−4574. (d) Gugliotta, G.; M. Botta, M.; Giovenzana, G. B.; Tei, L. *Bioorg. Med. Chem. Lett.* **2009**, *19*, 3442−3444.

(6) (a) Aime, S.; Botta, M.; Geninatti Crich, S.; Giovenzana, G.; Pagliarin, R.; Sisti, M.; Terreno, E. *Magn. Reson. Chem.* **1998**, *36*, S200−S208. (b) Thompson, M. K.; Botta, M.; Nicolle, G.; Helm, L.; Aime, S.; Merbach, A. E.; Raymond, K. N. *J. Am. Chem. Soc.* **2003**, *125*, 14274−14275. (c) Baranyai, Z.; Tei, L.; Giovenzana, G. B.; Kálmán, F. K.; Botta, M. *Inorg. Chem.* **2012**, *51*, 2597−2607. (d) Messeri, D.; Lowe, M. P.; Parker, D.; Botta, M. *Chem. Commun.* **2001**, 2742−2743. (e) Werner, E. J.; Datta, A.; Jocher, C. J.; Raymond, K. N. *Angew. Chem., Int. Ed.* **2008**, *47*, 8568−8580. (f) Gale, E. M.; Kenton, N.; Caravan, P. *Chem. Commun.* **2013**, *49*, 8060−8062.

(7) (a) Geigy, J. R. GB Patent GB695346, 1953. (b) Mackey, J. L.; Hiller, M. A.; Powell, J. E. *J. Phys. Chem.* **1962**, *66*, 311−314.

(8) Baranyai, Z.; Botta, M.; Fekete, M.; Giovenzana, G. B.; Negri, R.; Tei, L.; Platas-Iglesias, C. *Chem.—Eur. J.* **2012**, *18*, 7680−7685.

(9) Anderegg, G. *Helv. Chim. Acta* **1964**, *47*, 1801−1814.

(10) Martell, A. E.; Smith, R. M. *Critical stability constants*; Plenum Press: New York, 1974, 1982; Vols. *1*−*5*.

(11) Baranyai, Z.; Palinkas, Z.; Uggeri, F.; Brucher, E. *Eur. J. Inorg. Chem.* **2010**, 1948.

(12) Regueiro-Figueroa, M.; Esteban-Gomez, D.; de Blas, A.; Rodriguez-Blas, T.; Platas-Iglesias, C. *Chem.—Eur. J.* **2014**, *20*, 3974−3981.

(13) Baranyai, Z.; Palinkas, Z.; Uggeri, F.; Maiocchi, A.; Aime, S.; Brucher, E. *Chem.—Eur. J.* **2012**, *18*, 16426−16435.

(14) Sarka, L.; Burai, L.; Brucher, E. *Chem.—Eur. J.* **2000**, *6*, 719−724.

(15) Eigen, M. *Angew. Chem., Int. Ed. Engl.* **1964**, *3*, 1−19.

(16) Janicki, R.; Mondry, A. *Eur. J. Inorg. Chem.* **2013**, 3429−3438.

(17) (a) Mato-Iglesias, M.; Rodríguez-Blas, T.; Platas-Iglesias, C.; Starck, M.; Kadjane, P.; Ziessel, R.; Charbonnière, L. *Inorg. Chem.* **2009**, *48*, 1507−1518. (b) Kadjane, P.; Platas-Iglesias, C.; Ziessel, R.; Charbonnière, L. *Dalton Trans.* **2009**, 5688−5700.

(18) Llunell, M.; Casanova, D.; Cirera, J.; Alemany, P.; Alvarez, S. *SHAPE. Program for the stereochemical analysis of molecular fragments by means of continuous shape measures and associated tools*, Version 2.1.

(19) (a) Pinsky, M.; Avnir, D. *Inorg. Chem.* **1998**, *37*, 5575−5582. (b) Ruíz-Martínez, A.; Casanova, D.; Alvarez, S. *Chem.—Eur. J.* **2008**, *14*, 1291−1303.

(20) Schauer, K. C.; Anderson, P. O. *J. Chem. Soc., Dalton Trans.* **1989**, 185−191.

(21) (a) Maigut, J.; Meier, R.; Zahl, A.; van Eldik, R. *Inorg. Chem.* **2008**, *47*, 5702−5719. (b) Maigut, J.; Meier, R.; Zahl, A.; van Eldik, R. *Inorg. Chem.* **2007**, *46*, 5361−5371.

(22) (a) Corey, E. J.; Bailar, J. C., Jr. *J. Am. Chem. Soc.* **1959**, *81*, 2620−2629. (b) Beattie, J. K. *Acc. Chem. Res.* **1971**, *4*, 253−259.

(23) Seitz, M.; Oliver, A. G.; Raymond, K. N. *J. Am. Chem. Soc.* **2007**, *129*, 11153−11160.

(24) Esteban-Gomez, D.; de Blas, A.; Rodriguez-Blas, T.; Helm, L.; Platas-Iglesias, C. *ChemPhysChem* **2012**, *13*, 3640−3650.

(25) (a) Regueiro-Figueroa, M.; Bensenane, B.; Ruscsák, E.; Esteban-Gómez, D.; Charbonnière, L. J.; Tircsó, G.; Tóth, I.; de Blas, A.; Rodríguez-Blas, T.; Platas-Iglesias, C. *Inorg. Chem.* **2011**, *50*, 4125−4141. (b) Purgel, M.; Baranyai, Z.; de Blas, A.; Rodríguez-Blas, T.; Bányai, I.; Platas-Iglesias, C.; Tóth, I. *Inorg. Chem.* **2010**, *49*, 4370−4382. (c) Regueiro-Figueroa, M.; Esteban-Gómez, D.; de Blas, A.; Rodríguez-Blas, T.; Platas-Iglesias, C. *Eur. J. Inorg. Chem.* **2010**, 3586−3595. (d) Natrajan, L. S.; Khoabane, N. M.; Dadds, B. L.; Muryn, C. A.; Pritchard, R. G.; Heath, S. L.; Kenwright, A. M.; Kuprov, I.; Faulkner, S. *Inorg. Chem.* **2010**, *49*, 7700−7709.

(26) (a) Di Vaira, M.; Stoppioni, P. *New J. Chem.* **2002**, *26*, 136−144. (b) Cosentino, U.; Villa, A.; Pitea, D.; Moro, G.; Barone, V.; Maiocchi, A. *J. Am. Chem. Soc.* **2002**, *124*, 4901−4909.

(27) (a) Jacques, V.; Desreux, J. F. *Inorg. Chem.* **1994**, *33*, 4048−4053. (b) Geraldes, C. F. G. C.; Urbano, A. M.; Hoefnagel, M. A.; Peters, J. A. *Inorg. Chem.* **1993**, *32*, 2426−2432. (c) Jenkins, B. G.; Lauffer, R. B. *Inorg. Chem.* **1988**, *27*, 4730−4738.

(28) Balogh, E.; Mato-Iglesias, M.; Platas-Iglesias, C.; Tóth, É.; Djanashvili, K.; Peters, J. A.; de Blas, A.; Rodríguez-Blas, T. *Inorg. Chem.* **2006**, *45*, 8719−8728.
(29) Aime, S.; Barge, A.; Borel, A.; Botta, M.; Chemerisov, S.; Merbach, A. E.; Müller, U.; Pubanz, D. *Inorg. Chem.* **1997**, *36*, 5104−5112.
(30) Beeby, A.; Clarkson, I. M.; Dickins, R. S.; Faulkner, S.; Parker, D.; Royle, L.; de Sousa, A. S.; Williams, J. A. G.; Woods, M. *J. Chem. Soc., Perkin Trans. 2* **1999**, 493−503.
(31) Powell, D. H.; Ni Dhubhghaill, O. M.; Pubanz, D.; Helm, L.; Lebedev, Y. S.; Schlaepfer, W.; Merbach, A. E. *J. Am. Chem. Soc.* **1996**, *118*, 9333−9346.
(32) (a) Banci, L.; Bertini, I.; Luchinat, C. *Nuclear and Electron Relaxation. The Magnetic Nucleus-Unpaired Electron Coupling in Solution*; VCH:Weinheim, Germany, 1991. (b) Bloembergen, N.; Morgan, L. O. *J. Chem. Phys.* **1961**, *34*, 842−850.
(33) (a) Hwang, L. P.; Freed, J. H. *J. Chem. Phys.* **1975**, *63*, 4017−4025. (b) Freed, J. H. *J. Chem. Phys.* **1978**, *69*, 4034−4037.
(34) (a) Swift, T. J.; Connick, R. E. J. *J. Chem. Phys.* **1962**, *37*, 307−312. (b) Powel, D. H. *J. Am. Chem. Soc.* **1996**, *118*, 9333−9346.
(35) Mills, R. *J. Chem. Phys.* **1973**, *77*, 658−688.
(36) Irving, H. M.; Miles, M. G.; Pettit, L. D. *Anal. Chim. Acta* **1967**, *38*, 475−488.
(37) Zékány, L., Nagypál, I. In *Computational Method for Determination of Formation Constants*; Legett, D. J., Ed.; Plenum: New York, 1985; p 291.
(38) (a) Becke, A. D. *J. Chem. Phys.* **1993**, *98*, 5648−5652. (b) Lee, C.; Yang, W.; Parr, R. G. *Phys. Rev. B* **1988**, *37*, 785−789.
(39) Frisch, M. J.; Trucks, G. W.; Schlegel, H. B.; Scuseria, G. E.; Robb, M. A.; Cheeseman, J. R.; Scalmani, G.; Barone, V.; Mennucci, B.; Petersson, G. A.; Nakatsuji, H.; Caricato, M.; Li, X.; Hratchian, H. P.; Izmaylov, A. F.; Bloino, J.; Zheng, G.; Sonnenberg, J. L.; Hada, M.; Ehara, M.; Toyota, K.; Fukuda, R.; Hasegawa, J.; Ishida, M.; Nakajima, T.; Honda, Y.; Kitao, O.; Nakai, H.; Vreven, T.; Montgomery, J. A., Jr.; Peralta, J. E.; Ogliaro, F.; Bearpark, M.; Heyd, J. J.; Brothers, E.; Kudin, K. N.; Staroverov, V. N.; Kobayashi, R.; Normand, J.; Raghavachari, K.; Rendell, A.; Burant, J. C.; Iyengar, S. S.; Tomasi, J.; Cossi, M.; Rega, N.; Millam, N. J.; Klene, M.; Knox, J. E.; Cross, J. B.; Bakken, V.; Adamo, C.; Jaramillo, J.; Gomperts, R.; Stratmann, R. E.; Yazyev, O.; Austin, A. J.; Cammi, R.; Pomelli, C.; Ochterski, J. W.; Martin, R. L.; Morokuma, K.; Zakrzewski, V. G.; Voth, G. A.; Salvador, P.; Dannenberg, J. J.; Dapprich, S.; Daniels, A. D.; Farkas, Ö.; Foresman, J. B.; Ortiz, J. V.; Cioslowski, J.; Fox, D. J. *Gaussian 09, Revision A.01*; Gaussian, Inc.: Wallingford, CT, 2009.
(40) Dolg, M.; Stoll, H.; Savin, A.; Preuss, H. *Theor. Chim. Acta* **1989**, *75*, 173−194.
(41) (a) Maron, L.; Eisestein, O. *J. Phys. Chem. A* **2000**, *104*, 7140−7143. (b) Eisestein, O.; Maron, L. *J. Organomet. Chem. A* **2002**, *647*, 190−197. (c) Adamo, C.; Maldivi, P. *Chem. Phys. Lett.* **1997**, *268*, 61−68. (d) Platas-Iglesias, C.; Roca-Sabio, A.; Regueiro-Figueroa, M.; Esteban-Gómez, D.; de Blas, A.; Rodríguez-Blas, T. *Curr. Inorg. Chem.* **2011**, *1*, 91−116.
(42) (a) Boehme, C.; Wipff, G. *J. Phys. Chem. A* **1999**, *103*, 6023−6029. (b) Boehme, C.; Wipff, G. *Inorg. Chem.* **1999**, *38*, 5734−5741. (c) Boehme, C.; Wipff, G. *Chem.—Eur. J.* **2001**, *7*, 1398−1407. (d) Denecke, M. A.; Rossberg, A.; Panak, P. J.; Weigl, M.; Schimmelpfennig, B.; Geist, A. *Inorg. Chem.* **2005**, *44*, 8418−8425. (e) Dobler, M.; Hirata, M.; Tachimori, S. *Phys. Chem. Chem. Phys.* **2003**, *5*, 2499−2504. (f) Georgieva, I.; Trendafilova, N.; Aquino, A. J. A.; Lischka, H. *Inorg. Chem.* **2007**, *46*, 10926−10936.
(43) Tomasi, J.; Mennucci, B.; Cammi, R. *Chem. Rev.* **2005**, *105*, 2999−3093.
(44) (a) Peng, C.; Ayala, P. Y.; Schlegel, H. B.; Frisch, M. J. *J. Comput. Chem.* **1996**, *17*, 49−56. (b) Peng, C.; Schlegel, H. B. *Isr. J. Chem.* **1994**, *33*, 449−454.
(45) Harms, K.; Wocadlo, S. *XCAD4*; University of Marburg: Marburg, Germany, 1995.
(46) Altomare, A.; Cascarano, G.; Giacovazzo, C.; Guagliardi, A. *J. Appl. Crystallogr.* **1993**, *26*, 343−350.
(47) Sheldrick, G. M. *Acta Crystallogr., Sect. A* **2008**, *64*, 112−122.
(48) Spek, A. *J. Appl. Crystallogr.* **2003**, *36*, 7−13.
(49) Farrugia, L. *J. Appl. Crystallogr.* **1999**, *32*, 837−838.